Earth and Planetary Science Letters 428 (2015) 193–203

Contents lists available at ScienceDirect

Earth and Planetary Science Letters

www.elsevier.com/locate/epsl

Antarctic Intermediate Water properties since 400 ka recorded in infaunal (*Uvigerina peregrina*) and epifaunal (*Planulina wuellerstorfi*) benthic foraminifera

Aurora C. Elmore [a,b,*], Erin L. McClymont [a], Henry Elderfield [b], Sev Kender [c,d], Michael R. Cook [b], Melanie J. Leng [e,c], Mervyn Greaves [b], Sambuddha Misra [b]

[a] Department of Geography, Durham University, Durham, UK
[b] Earth Sciences Department, University of Cambridge, Cambridge, UK
[c] Centre for Environmental Geochemistry, School of Geography, University of Nottingham, Nottingham, UK
[d] British Geological Survey, Keyworth, Nottingham, UK
[e] NERC Isotope Geosciences Facilities, British Geological Survey, Keyworth, Nottingham, UK

ARTICLE INFO

Article history:
Received 21 August 2014
Received in revised form 30 June 2015
Accepted 6 July 2015
Available online 3 August 2015
Editor: J. Lynch-Stieglitz

Keywords:
Antarctic Intermediate Water
Deep Sea Drilling Program Site 593
benthic foraminifera
stable isotopes
Mg/Ca
B/Ca

ABSTRACT

Reconstruction of intermediate water properties is important for understanding feedbacks within the ocean-climate system, particularly since these water masses are capable of driving high–low latitude teleconnections. Nevertheless, information about intermediate water mass evolution through the late Pleistocene remains limited. This paper examines changes in Antarctic Intermediate Water (AAIW), the most extensive intermediate water mass in the modern ocean through the last 400 kyr using the stable isotopic composition ($\delta^{18}O$ and $\delta^{13}C$) and trace element concentration (Mg/Ca and B/Ca) of two benthic foraminiferal species from the same samples: epifaunal *Planulina wuellerstorfi* and infaunal *Uvigerina peregrina*. Our results confirm that the most reasonable estimates of AAIW temperature and $\Delta[CO_3^{2-}]$ are generated by $Mg/Ca_{U.\ peregrina}$ and $B/Ca_{P.\ wuellerstorfi}$, respectively. We present a 400 kyr record of intermediate water temperature and $\Delta[CO_3^{2-}]$ from a sediment core from the Southwest Pacific (DSDP site 593; 40°30′S, 167°41′E, 1068 m water depth), which lies within the core of modern AAIW. Our results suggest that a combination of geochemical analyses on both infaunal and epifaunal benthic foraminiferal species yields important information about this critical water mass through the late Pleistocene. When combined with two nearby records of water properties from deeper depths, our data demonstrate that during interglacial stages of the late Pleistocene, AAIW and Circumpolar Deep Water (CPDW) have more similar water mass properties (temperature and $\delta^{13}C$), while glacial stages are typified by dissimilar properties between AAIW and CPDW in the Southwest Pacific. Our new $\Delta[CO_3^{2-}]$ record shows short time-scale variations, but a lack of coherent glacial–interglacial variability indicating that large quantities of carbon were not stored in intermediate waters during recent glacial periods.

1. Introduction

The Southern Ocean is a critical component of the ocean-climate system since it is capable of substantial carbon storage and variable CO_2 fluxes across the air–sea interface (Burke and Robinson, 2012; Anderson et al., 2009). The deep Southern Ocean contains waters sourced near Antarctica, and proximal sediment core records of benthic foraminiferal Mg/Ca (Martin et al., 2002; Elderfield et al., 2010) and stable isotopes (McCave et al., 2008) indicate that the deep Southern Ocean was cooler during glacial stages than during interglacials of the late Pleistocene. Glacial stages are also characterized by increased export of less-ventilated southern-sourced waters to the deep Pacific Ocean via Circumpolar Deep Water (CPDW; e.g., Hall et al., 2001; McCave et al., 2008). Above these deep Pacific waters, Antarctic Intermediate Water (AAIW) also forms in the high southern latitudes of the Pacific Ocean, in association with the Subantarctic Front (Reid, 1997; Herraiz-Borreguero and Rintoul, 2011; Fig. 1). AAIW is a globally important water mass since it extends to 20°N in the Atlantic, Pacific, and Indian Oceans, making it one of the largest water masses in the modern ocean (Talley, 1999; Bostock et al., 2010, 2013b). Since AAIW feeds waters that upwell in the tropics and subtropics,

* Corresponding author at: Department of Geography, Durham University, Science Site, South Rd, Durham, DH1 3LE, UK. Tel.: +44 (0) 191 33 41931.
E-mail address: aurora.elmore@durham.ac.uk (A.C. Elmore).

http://dx.doi.org/10.1016/j.epsl.2015.07.013

Table 1
Location and water depth of cores used in this study.

Core name	Latitude	Longitude	Water depth (m)	Reference
DSDP593	40°30.47′S	167°40.47′E	1068	This study
MD97-2120	45°32.06′S	174°55.85′W	1210	Pahnke and Zahn, 2005; Cook, 2009
ODP1123	41°47.15′S	171°29.94′W	3290	Elderfield et al., 2010, 2012

it provides a physical link between the high- and low-latitudes, transporting heat, salt, and nutrients to these regions (Reid, 1997). As a reflection of stratification and sea-ice extent in the Southern Ocean, observing AAIW properties can provide potentially important insights into oceanic CO_2 storage, upwelling, and atmospheric exchange during recent deglaciations (e.g. Anderson et al., 2009).

Despite the key role of AAIW at a range of temporal and spatial scales in the modern ocean, little is known about the long-term interaction of this water mass with global climate due to a lack of critical proxy data (Pahnke et al., 2003; Pahnke and Zahn, 2005). Pacific intermediate water convection was likely deeper (~2 km) and more intense during the last glacial period, but whether this had a northern or southern source (or both) is not yet resolved (Basak et al., 2010). In contrast, Marchitto et al. (2007) argued that AAIW was at times fed by deep overturning circulation in the Southern Ocean during millennial-scale climate events. Analysis of millennial-scale climate variability during the late Pleistocene demonstrates the potential for AAIW to be a driver in high–low latitude teleconnections on shorter time scales owing to transportation of heat and storage of CO_2 (Bostock et al., 2010; Pahnke and Zahn, 2005). Understanding intermediate water properties during large climatic transitions and on shorter timescales will further our understanding of drivers and feedbacks of past climate changes during the late Pleistocene. However, generating these records is complicated due to the limited development of geochemical proxies at intermediate water depths.

We examine changes in two AAIW properties through the late Pleistocene using benthic foraminiferal stable isotopic and trace elemental ratios to characterize the intermediate waters that are exported from the Southern Ocean to the Pacific. We focus on the reconstruction of AAIW temperature and carbonate ion concentration, since these properties give insights into Southern Ocean circulation and atmospheric CO_2 exchange (Bostock et al., 2010, 2013b; Rae et al., 2011; Allen et al., 2015). Specifically, we investigate the differences between epifaunal (*Planulina wuellerstorfi*) and infaunal (*Uvigerina peregrina*) foraminiferal $\delta^{18}O$, $\delta^{13}C$, Mg/Ca, and B/Ca at an intermediate water depth site. We investigate: 1) if the $Mg/Ca_{U.\ peregrina}$ paleotemperature proxy (Elderfield et al., 2010) is viable and devoid of carbonate ion effects at intermediate water depths; 2) the utility of $B/Ca_{U.\ peregrina}$ to reconstruct past changes in intermediate water $\Delta[CO_3^{2-}]$; and 3) changes to the paleoceanographic history of AAIW over the last 400 kyr.

2. Location, materials, and methods

2.1. Study site

Hole DSDP593Z (40°30′S, 167°41′E, 1068 m water depth) lies to the north of the modern Subtropical Front (STF) within the Tasman Sea, and is presently bathed by AAIW, which extends to a depth of ~1500 m (Fig. 1A). Modern hydrography at DSDP593 (Fig. 1B) is complicated by variable regional bathymetry and mixing of interior water masses, examined in depth by Bostock et al. (2013a, 2013b). Relatively fresh, well-oxygenated, low-nutrient, and young Southern Ocean-sourced AAIW forms near the Subantarctic Front (SAF) and flows to the north below 500 m to

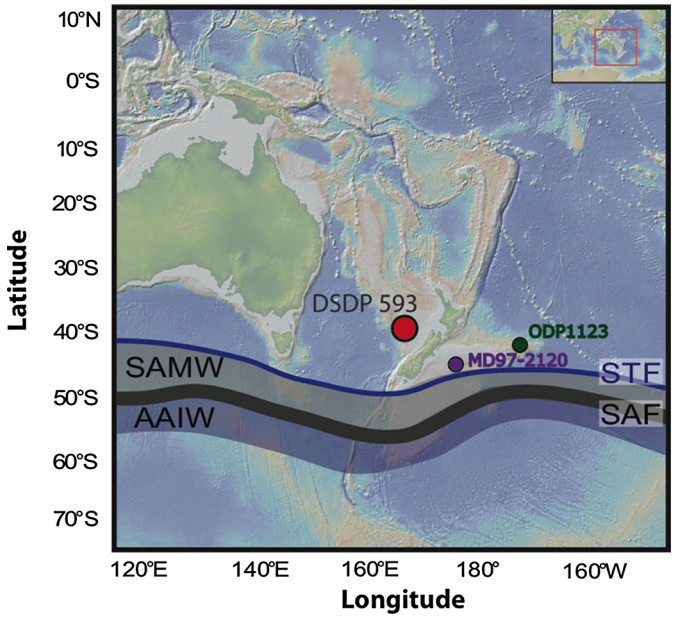

Fig. 1A. Site location of marine sediment cores DSDP593 (red; 40°30′S, 167°41′E, 1068 m water depth), MD97-2120 (purple; 45°32′S, 174°56′E, 1210 m water depth), and ODP1123 (green; 41°47′S, 171°30′W, 3290 m water depth). Locations of the Subtropical Front (STF; blue) and Subantarctic Front (SAF), which define the formation regions for Subantarctic Mode Water (SAMW), Antarctic Intermediate Water (AAIW) are also shown. (For interpretation of the references to color in this figure, the reader is referred to the web version of this article.)

the east and west of New Zealand (Bostock et al., 2013b; see supplement Section 1). Intermediate waters at DSDP593 are primarily Southern-sourced AAIW, with possible mixing of thermocline waters from the Tasman Sea providing a minor contribution from the north (Herraiz-Borreguero and Rintoul, 2011; Bostock et al., 2013b). Owing to the proximity of our study location to the STF and SAF, variations in surface currents and winds (i.e. the Westerlies) may have a large control on the formation regions of AAIW at our site. Present hydrographic conditions at DSDP593 are 34.5–34.6 PSU, bottom water temperature 4–5 °C (Schlitzer, 2002; Mulhearn, 1985), and modern $\Delta[CO_3^{2-}]$ is estimated at 34 μmol/kg (see supplement Section 1) (Table 1).

2.2. Age model

The late Quaternary section of core DSDP593 is continuous (without splices or gaps) and is foraminifer-bearing to foraminifer nannofossil ooze according to the original site report (Nelson, 1986); the abundant, well-preserved foraminifera have enabled previous palaeoceanographic studies (e.g., Cooke et al., 2004; Head and Nelson, 1994). An approximate age model was obtained from shipboard chrono-stratigraphic tie points (Kennett et al., 1986) and coarse resolution benthic foraminiferal $\delta^{18}O_{U.\ peregrina}$ (Nelson et al., 1986; Head and Nelson, 1994), which allowed for targeted sampling of glacial and interglacial intervals. The top ~7.75 m contains sediments recording the last ~400 kyr, yielding average sedimentation rate of ~1.9 cm/kyr (see supplement Section 1). Samples in this section were 2 cm wide and taken approximately every 8 cm, yielding a sampling resolution of ~4 kyr. Higher resolution sampling was prohibited by availability and the brittle nature of sediments at the time of sampling in 2010 and 2011. Our $\delta^{18}O_{P.\ wuellerstorfi}$ record (see Section 2.3) was used to generate a new age model by visually comparing to the global $\delta^{18}O$ stack of Lisiecki and Raymo (2005). Chrono-stratigraphic tie points were determined by assigning the maxima and minima values of benthic foraminiferal $\delta^{18}O$ to glacials and interglacials, respectively. Addi-

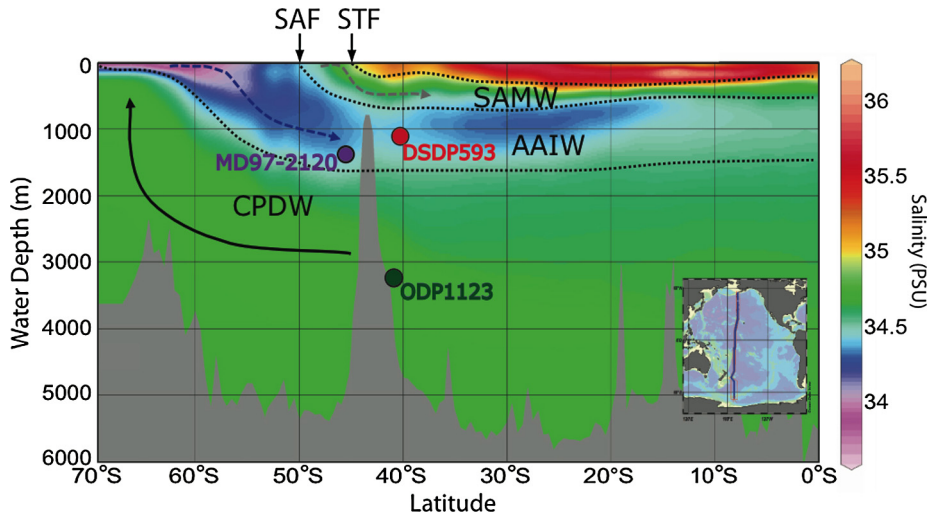

Fig. 1B. Location of sites DSDP593 (red), MD97-2120 (purple), and ODP1123 (green) projected on to WOCE hydrographic section P15 (see inset) of salinity from Schlitzer (2002). The location of the Subantarctic Front (SAF) and Subtropical Front (STF) are shown, as well as interior water masses; Subantarctic Mode Water (SAMW), Antarctic Intermediate Water (AAIW), and Circumpolar Deep Water (CPDW, including Antarctic Bottom Water; after Elderfield et al., 2010). (For interpretation of the references to color in this figure, the reader is referred to the web version of this article.)

tional chrono-stratigraphic tie points came from a radiocarbon date at 0.31 mbsf (15.9 ka; Nelson, 1986) and the Brunhes/Matuyama boundary at 16.30 mbsf (780 ka; Dudley and Nelson, 1989). All ages were linearly interpolated between tie points (see supplement Section 1 for age–depth tie points).

2.3. Stable isotopic and trace elemental analyses

Approximately 10 cc of sediment from the selected intervals was oven dried overnight at 40 °C, and washed with deionized water through a 63 μm sieve. The >63 μm fraction was dried again and individual species of foraminifera were hand-picked under a binocular microscope. From each sample, 4 *P. wuellerstorfi* tests were selected from the >250 μm fraction for $\delta^{18}O$ and $\delta^{13}C$ analyses by IsoPrime dual inlet mass spectrometer with Multiprep device at the NERC Isotope Geosciences Laboratory. ^{13}C and ^{18}O are reported as per mille (‰) deviations of isotopic ratios ($^{13}C/^{12}C$, $^{18}O/^{16}O$), calculated to the V-PDB scale using a within-run laboratory standard calibrated against NBS-19 standards. Analytical reproducibility of an in-house calcite standard (KCM) is <0.1‰ for both $\delta^{13}C$ and $\delta^{18}O$ during this study. Specific attention was paid to select the most characteristic individuals as different morphotypes of *Planulina*/*Cibicidoides* yield offsets in stable isotopic composition (e.g., Elmore, 2009). All previously unpublished data is available online at: https://www.ncdc.noaa.gov/paleo/study/18918.

Approximately 10 individuals of benthic foraminifera *U. peregrina* and *P. wuellerstorfi* were selected from the >250 μm fraction to yield monospecific samples. The foraminifera were chosen for their pristine appearance (i.e., white calcite, no visible adhered clays, no visible recrystallization), and particular attention was paid to species morphotypes, as *Planulina*/*Cibicidoides* have species-specific elemental fractionation (Yu and Elderfield, 2007; Rae et al., 2011). Mixed *Uvigerina* species have been previously used for elemental analysis (Yu and Elderfield, 2007; Elderfield et al., 2010; Rae et al., 2011); however, only *U. peregrina* was used in this study as *Uvigerina* species may have variable depth habitats and thus incorporate elements differently (Linda Booth, personal communication), possibly owing to differing depth habitats among *Uvigerina* species (Williams et al., 1988). For elemental concentrations, benthic foraminifera were cleaned following the oxidative procedure of Barker et al. (2003), and analyzed for Mg/Ca and B/Ca by ICP-OES and ICP-MS, respectively, at the Godwin Laboratory for Palaeoclimate Research, University of Cambridge. All analyzed tests appeared visually well preserved, and Fe/Ca and Mn/Ca measurements indicate that samples were effectively cleaned and devoid of diagenetic effects (see supplement Section 2).

2.4. Estimations of intermediate water temperature and calcite saturation state

Four separate estimations of past intermediate water temperatures (IWT) were generated from DSDP593 foraminiferal geochemical data to determine the best method of estimating IWT at our site (see supplement Section 3 for additional information on these calculations). For estimating temperature from $\delta^{18}O_{calcite}$, a global seawater ($\delta^{18}O_{sw}$) record was generated by linearly scaling a sea level record from Rohling et al. (2009; see supplement Section 2) according to the global Last Glacial Maximum to Holocene $\delta^{18}O_{sw}$ change of 1.05‰ from Schrag et al. (2002). No additional correction was applied for initial regional $\delta^{18}O_{sw}$ because the modern $\delta^{18}O_{sw}$ data from the closest available location to DSDP593 (38°23′S, 170°04′E, 1088 m water depth; Ostlund et al., 1987) is 0.01‰, which is within the average analytical error from our foraminiferal $\delta^{18}O$ analyses. This method presumes no change in local $\delta^{18}O_{sw}$ beyond the global ice volume effect. Temperatures were then estimated according to the species-specific calibrations from Marchitto et al. (2014) using our data from *P. wuellerstorfi* and previously published $\delta^{18}O_{U.\ peregrina}$ data from (Head and Nelson, 1994):

$$\delta^{18}O_{P.\ wuellerstorfi} - \delta^{18}O_{sw} + 0.27‰ = -0.225\ \mathrm{IWT} + 3.5 \quad (1)$$

$$\delta^{18}O_{U.\ peregrina} - \delta^{18}O_{sw} + 0.27‰ = -0.207\ \mathrm{IWT} + 3.75 \quad (2)$$

An additional IWT estimate was made by applying the warm water calibration for epifaunal $Mg/Ca_{Cibicidoides}$ from Elderfield et al. (2006), which suggests that the Carbonate Ion Effect is weaker at warmer temperatures, such as our intermediate depth site:

$$Mg/Ca_{Cibicidoides} = 0.90 \exp(0.11\ \mathrm{IWT}) \quad (3)$$

Finally, the most recent published calibration for estimating IWT from infaunal $Mg/Ca_{U.\ peregrina}$, from Elderfield et al. (2010; 2012), has proposed that the infaunal habitat of *Uvigerina* yields a carbonate ion-independent temperature–Mg/Ca relationship:

$$Mg/Ca_{U.\ peregrina} = 0.1 * \mathrm{IWT} + 1.0\ \mathrm{mmol/mol} \quad (4)$$

Three methods are available to calculate intermediate water calcite saturation state ($\Delta[CO_3^{2-}]$; defined as the difference between $[CO_3^{2-}]_{in\ situ}$ and $[CO_3^{2-}]_{saturation}$, the latter being 56 µmol/kg at our site) using foraminiferal geochemistry from DSDP593 (see supplement Section 3 for additional information). Firstly, Yu and Elderfield (2008) proposed that carbonate ion concentration controls $Mg/Ca_{P.\ wuellerstorfi}$ according to the equation:

$$Mg/Ca_{P.\ wuellerstorfi} = 0.0108 * \Delta[CO_3^{2-}] + 0.99\ \text{mmol/mol} \quad (5)$$

Additionally, the B/Ca ratio of infaunal *Uvigerina*, which has a low concentration of boron (Misra et al., 2014) has yielded no robust published $\Delta[CO_3^{2-}]$ calibrations; a linear relationship has been suggested by Doss (2014), corroborating an earlier, preliminary study by Rae et al. (2011):

$$B/Ca_{U.\ peregrina} = 0.25 \pm 0.015 * \Delta[CO_3^{2-}] + 18.3 \pm 0.304\ \mu\text{mol/mol} \quad (6)$$

Lastly, the B/Ca ratio of epifaunal foraminifera *P. wuellerstorfi* has been related to $\Delta[CO_3^{2-}]$ and has been previously applied in our study region (Allen et al., 2015) using the established calibration from Rae et al. (2011):

$$B/Ca_{P.\ wuellerstrorfi} = 1.14 \pm 0.048 * \Delta[CO_3^{2-}] + 177.1 \pm 1.41\ \mu\text{mol/mol} \quad (7)$$

3. Results and discussion

3.1. Proxies for estimating past intermediate water temperatures

Validation of paleoceanographic proxies is typically achieved using core top calibrations (e.g., Rae et al., 2011; Elderfield et al., 2010), however multiple downcore proxy records from the same site can also provide valuable information about the validity of proxies. Herein, to evaluate each of the following proxies using our new downcore data, we first compare the measured coretop (late Holocene) proxy value to the modern oceanic parameters. We also examine the maxima and minima of the proxy record to determine if the values are oceanographically plausible. Lastly, we can compare proxies against other, established proxies from the same site and/or nearby sites.

Estimations of past IWT rely on stable isotopic or trace element foraminiferal chemistry; while both infaunal and epifaunal benthic foraminiferal species have been used in previous paleoceanographic studies (e.g., Head and Nelson, 1994; Elderfield et al., 2010), our estimations of IWT from DSDP593 reveal differences between $\delta^{18}O$ of infaunal and epifaunal species. Over the past 400 kyr, epifaunal $\delta^{18}O_{P.\ wuellerstorfi}$ values from DSDP593 oscillate between +2.2‰ during interglacials and +3.7‰ during glacial minima (Fig. 2A), according to the typical 'saw-tooth pattern' (Lisiecki and Raymo, 2005), reflecting the global, orbital pacing of the ice ages. However, interglacial Marine Isotope Stages (MIS) 9 and 7.3–7.1 have $\delta^{18}O_{P.\ wuellerstorfi}$ values of ∼ +3.0‰, and ∼ +3.3‰, respectively, which are higher than other interglacial minima during the interval of study (Fig. 2A). When used to estimate IWT at DSDP593, $\delta^{18}O_{P.\ wuellerstorfi}$ (this study) and $\delta^{18}O_{U.\ peregrina}$ (Head and Nelson, 1994), both yield a late Holocene IWT of ∼ 1 °C, which is significantly lower than modern recorded IWT (>4 °C; Schlitzer, 2002). Additionally, during the interval from 400-0 ka, the IWT estimates from both species reach as low as −1 °C (MIS 2, 5A, and 6 for *U. peregrina* and MIS 6 for *P. wuellerstorfi*; Fig. 2B). This minimum IWT is unrealistic given the water depth (1068 m) and the fact that the freezing temperature of seawater is ∼ −2 °C, thus if glacial IWT were below 0 °C, typical temperature gradients to the deep ocean would require a mostly frozen deep ocean. However, for the majority of the record, both species give reasonable IWT estimates. These estimations of IWT from benthic foraminiferal $\delta^{18}O$ do not include local/regional salinity variations that can also contribute to $\delta^{18}O_{sw}$. Some of the glacial–interglacial temperature difference estimated from the $\delta^{18}O$ of both benthic species (Fig. 2B) is therefore likely due to changes in salinity of the water mass bathing DSDP593, necessitating saltier intermediate waters during glacial periods. This salinity issue may partially explain the poor relationship between IWT derived from both species $\delta^{18}O$ and the established paleotemperature proxy $Mg/Ca_{U.\ peregrina}$ (Fig. 3D).

Estimations of IWT from foraminiferal Mg/Ca ratios from DSDP593 show differing downcore trends when compared to the IWT estimates from $\delta^{18}O$ (Fig. 2B) and thus demonstrate further differences between the infaunal and epifaunal benthic species. The $Mg/Ca_{P.\ wuellerstorfi}$ ratio is generally higher during interglacials than glacials, indicating warmer interglacials, as expected. However, $Mg/Ca_{P.\ wuellerstorfi}$ appears to consistently overestimate IWT since the entirety of the 400-kyr record, including past glacial intervals, has temperatures from 4.0–7.5 °C ($Mg/Ca_{P.\ wuellerstorfi}$ = 1.4–2.1 mmol/mol; Fig. 2B). It is highly unlikely that past glacial AAIW was warmer than modern conditions (>4 °C; Schlitzer, 2002), therefore $Mg/Ca_{P.\ wuellerstorfi}$ is not a suitable proxy for IWT in this location using currently available paleotemperature calibrations.

Finally, the coretop IWT estimate (3.5 °C) from $Mg/Ca_{U.\ peregrina}$ (∼1.35 mmol/mol) is the most similar to the recorded modern temperature at DSDP593, >4 °C (Schlitzer, 2002). $Mg/Ca_{U.\ peregrina}$ shows an imperfect glacial–interglacial structure with warmer interglacials (∼3.5 °C; $Mg/Ca_{U.\ peregrina}$ = 1.5 mmol/mol) and cooler glacials (∼1.0 °C; $Mg/Ca_{U.\ peregrina}$ = 1.2 mmol/mol; Fig. 2B). A lack of $\Delta[CO_3^{2-}]$ control on $Mg/Ca_{U.\ peregrina}$, as suggested by Elderfield et al. (2010), is confirmed by the poor correlation between $Mg/Ca_{U.\ peregrina}$ and $B/Ca_{P.\ wuellerstorfi}$, the latter being an established proxy for $\Delta[CO_3^{2-}]$ (Rae et al., 2011), both in down core trend (Fig. 2C) and in cross plot ($R^2 = 0.00151$; Fig. 3A). Additionally, a weak correlation between $Mg/Ca_{P.\ wuellerstorfi}$ and $Mg/Ca_{U.\ peregrina}$ in cross plot ($R^2 = 0.02035$; Fig. 3B) implies that there are different controls on the Mg/Ca of the two species, either via species-specific magnesium incorporation and/or post-depositional effects. These results are supported by coretop calibration studies that indicate a secondary control (i.e., Carbonate Ion Effect) on $Mg/Ca_{P.\ wuellerstorfi}$ (Elderfield et al., 2006; Yu and Elderfield, 2008), which is not observed in $Mg/Ca_{U.\ peregrina}$ (Elderfield et al., 2010). Therefore, we maintain that the best estimates of past IWT at DSDP593 are achieved by using $Mg/Ca_{U.\ peregrina}$ (Fig. 2B).

3.2. Proxies for estimating past intermediate water carbonate saturation state

As with the available IWT proxies, there are several methods by which foraminiferal geochemistry can be used to approximate the past carbonate saturation state of seawater (e.g., Yu and Elderfield, 2007; Rae et al., 2011; Raitzsch et al., 2011). Three methods for estimating $\Delta[CO_3^{2-}]$ from benthic foraminiferal geochemistry from DSDP593 show differing trends over the past 400 kyr providing insight into the utility of these proxies at intermediate water depths (Fig. 2C). Using the calibration of Yu and Elderfield (2008) for $Mg/Ca_{P.\ wuellerstorfi}$, the entire 400-kyr record at DSDP593 yields $\Delta[CO_3^{2-}]$ values that range between 60–110 µmol/kg, which are uniformly higher than the modern estimate of 34 µmol/kg. This scenario does not align with estimates of $\Delta[CO_3^{2-}]$ from another intermediate-depth (∼1607 m) Southern Ocean-proximal site, which records $\Delta[CO_3^{2-}]$ values that are both higher and lower than modern over the last deglaciation (Allen et al., 2015). Therefore,

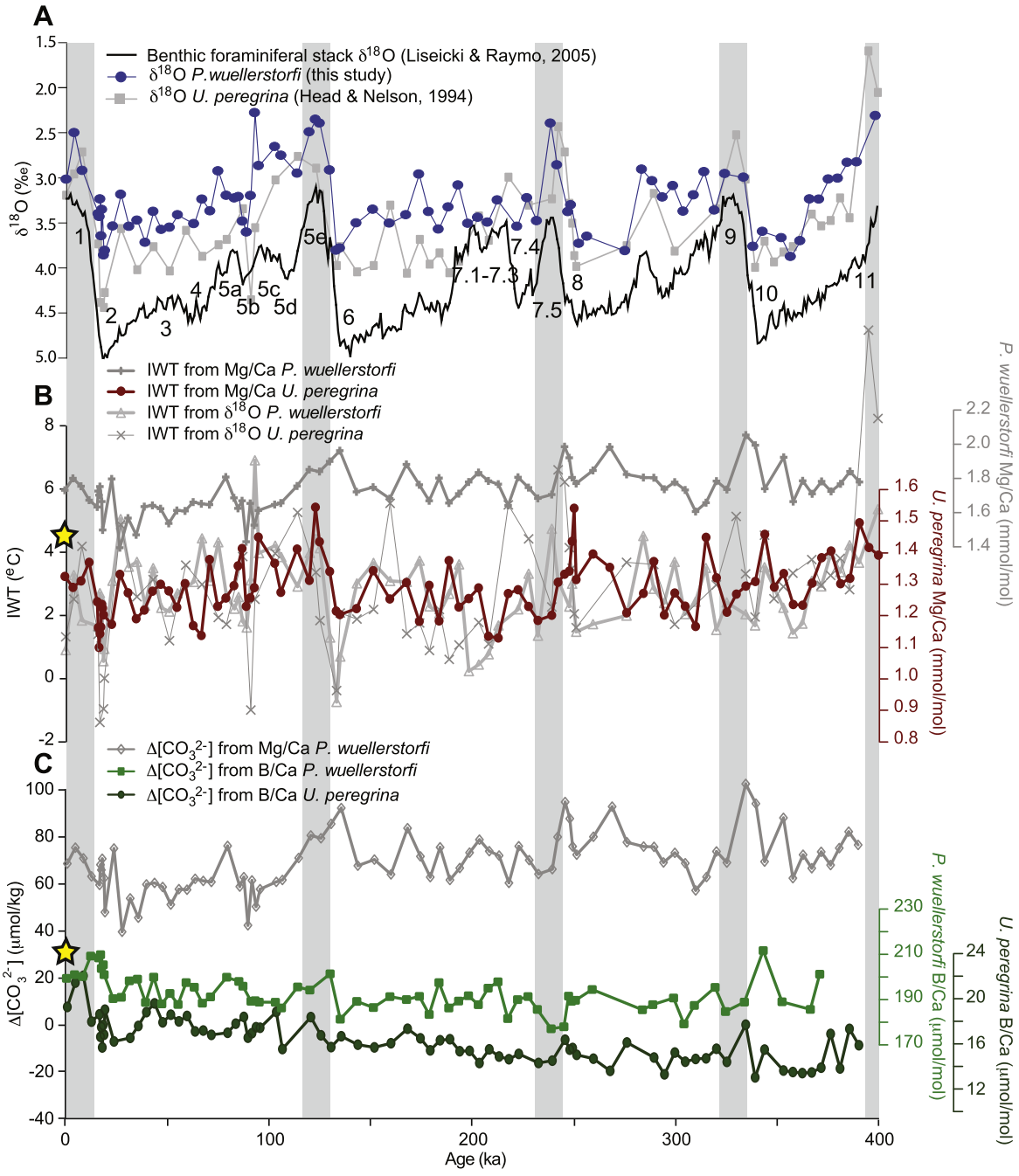

Fig. 2. A: Downcore data from DSDP593 showing our new $\delta^{18}O_{P.\ wuellerstorfi}$ data (blue circles) and previously published $\delta^{18}O_{U.\ peregrina}$ data from the same core (grey squares; Head and Nelson, 1994) with LR04 stack (black line). Interglacial stages are identified by odd numbers according to Lisiecki and Raymo (2005) and are highlighted by grey bars; glacial stages are identified by even numbers. B: Comparison of intermediate water temperature (IWT) estimates generated from DSDP593, $\delta^{18}O_{P.\ wuellerstorfi}$ (grey triangle; estimated according to species-specific calibrations in Marchitto et al., 2014, using $\delta^{18}O_{sw}$ estimated from Rohling et al., 2009 and without taking local salinity into effect), $\delta^{18}O_{U.\ peregrina}$ (grey 'x'; estimated as above using data previously published by Head and Nelson, 1994), $Mg/Ca_{P.\ wuellerstorfi}$ (grey crosses; according to Elderfield et al., 2006), and $Mg/Ca_{U.\ peregrina}$ (maroon; according to Elderfield et al., 2010). Modern bottom water temperature at DSDP593 is 4–5 °C, shown by the yellow star (Dudley and Nelson, 1989). C: Comparison of DSDP593 paleo-$\Delta[CO_3^{2-}]$ records generated from $Mg/Ca_{P.\ wuellerstorfi}$ (grey diamond; according to Yu and Elderfield, 2008), $B/Ca_{P.\ wuellerstorfi}$ (green squares; according to Rae et al., 2011), and $B/Ca_{U.\ peregrina}$ (dark green circles; according to Doss, 2014). Modern $\Delta[CO_3^{2-}]$ is ~34 µmol/kg, shown by the yellow star (see methods section). (For interpretation of the references to color in this figure, the reader is referred to the web version of this article.)

this indicates that $Mg/Ca_{P.\ wuellerstorfi}$ does not acceptably record $\Delta[CO_3^{2-}]$ at our site (Fig. 2C). Further, the poor correspondence ($R^2 = 0.15945$) between $Mg/Ca_{P.\ wuellerstorfi}$ and an established proxy for $\Delta[CO_3^{2-}]$, $B/Ca_{P.\ wuellerstorfi}$ (Rae et al., 2011), indicates that $\Delta[CO_3^{2-}]$ is not the dominant control on $Mg/Ca_{P.\ wuellerstorfi}$ (Fig. 3C).

A second proposed proxy for carbonate saturation state, infaunal $B/Ca_{U.\ peregrina}$ (Doss, 2014), shows a general increasing trend from 400–0 ka, with values ranging from ~14 µmol/mol ($\Delta[CO_3^{2-}] = \sim -22$ µmol/kg) during MIS 10, to ~23 µmol/mol ($\Delta[CO_3^{2-}] = \sim 20$ µmol/kg) during MIS 1 (Fig. 2C). Some glacial–interglacial variability is superimposed on the long-term trend, with slightly higher values recorded during interglacials, especially during MIS 1 (Fig. 2C). The coretop $B/Ca_{U.\ peregrina}$ method (8 µmol/kg) underestimates the modern $\Delta[CO_3^{2-}]$ value of 34 µmol/kg by more than the errors in the calibration. Further, the $B/Ca_{U.\ peregrina}$ would suggest that there was no time (glacial or

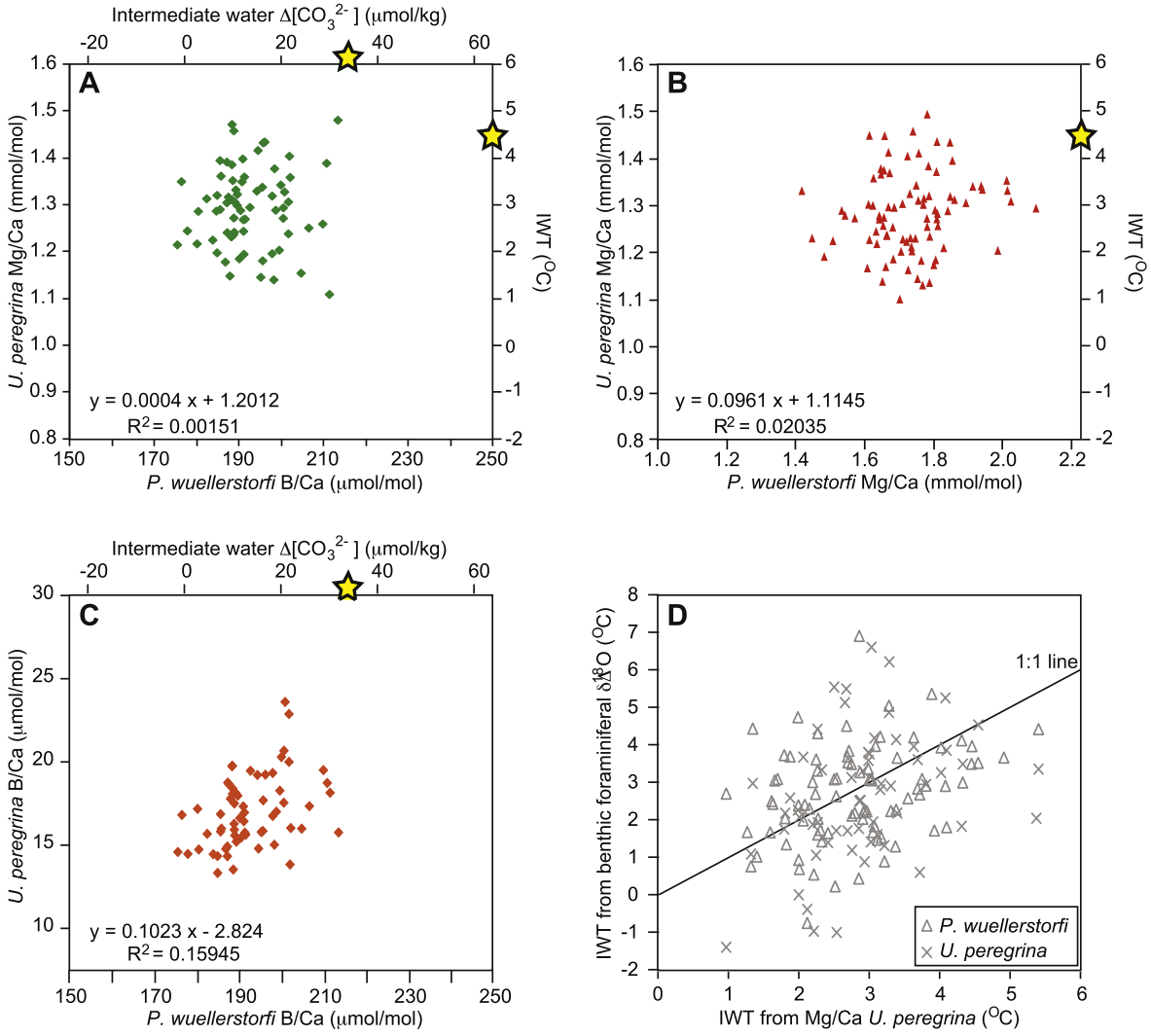

Fig. 3. Cross plots of elemental ratios from 0–400 ka from DSDP593. A: $Mg/Ca_{U.\ peregrina}$ and $B/Ca_{P.\ wuellerstorfi}$, where $B/Ca_{P.\ wuellerstorfi}$ has been shown to be dependent on carbonate ion (e.g., Rae et al., 2011), therefore the lack of relationship above ($R^2 = 0.00151$) demonstrates that $Mg/Ca_{U.\ peregrina}$ is independent of carbonate ion concentration over the estimated temperature range of 0–5 °C, according to the temperature calibration of Elderfield et al. (2010). Modern values for IWT and $\Delta[CO_3^{2-}]$ are indicated by yellow stars. B: Cross plot of $Mg/Ca_{U.\ peregrina}$ versus $Mg/Ca_{P.\ wuellerstorfi}$ shows no correlation between temperature-controlled $Mg/Ca_{U.\ peregrina}$ and carbonate ion-effected $Mg/Ca_{P.\ wuellerstorfi}$. C: Cross plot of $B/Ca_{U.\ peregrina}$ and carbonate ion-controlled $B/Ca_{P.\ wuellerstorfi}$ shows a weak correlation ($R^2 = 0.15945$). D: Cross plot of intermediate water temperature (IWT) from $Mg/Ca_{U.\ peregrina}$ versus IWT calculated from $\delta^{18}O$ of two species of benthic foraminifera, epifaunal *P. wuellerstorfi* (triangles) and infaunal *U. peregrina* (×). Both species show poor correlation with the Mg/Ca IWT data as evidenced by the scatter around a theoretical 1:1 correlation line. (For interpretation of the references to color in this figure, the reader is referred to the web version of this article.)

interglacial) in the last 400 kyr where $\Delta[CO_3^{2-}]$ approximated modern values, which again is unrealistic (Fig. 2C). As with the unexplained offset between $\delta^{18}O_{U.\ peregrina}$ and equilibrium bottom water chemistry (e.g., Marchitto et al., 2014), the long term increase in $B/Ca_{U.\ peregrina}$ is likely due to the infaunal nature of the species; it is possible that changing organic carbon inputs or sedimentation of other biogenic calcite have affected the pore water chemistry over time (Fig. 2C).

Finally, epifaunal $B/Ca_{P.\ wuellerstorfi}$ ranges in value from 175–215 μmol/mol during the interval from 400–0 ka, and does not have a longer-term increasing trend ($\Delta[CO_3^{2-}] = \sim$0–35 μmol/kg; Fig. 2C). Estimation of $\Delta[CO_3^{2-}]$ from $B/Ca_{P.\ wuellerstorfi}$ yields a Holocene value of ~20 μmol/kg, which still underestimates the modern value (34 μmol/kg), though this method comes closest to approximating the modern value. Despite limited data availability in the earlier part of the record, $B/Ca_{P.\ wuellerstorfi}$ does not show a coherent saw-toothed pattern of glacial and interglacial transitions (Fig. 2C). Interglacial $B/Ca_{P.\ wuellerstorfi}$ values are lower during the MIS 7 and 9, though the values are inconsistent among the interglacials, and MIS 1 and 5e record higher $B/Ca_{P.\ wuellerstorfi}$ values (Fig. 2C). Higher $B/Ca_{P.\ wuellerstorfi}$ values are observed during some transitions from glacials to interglacials, with the highest overall values recorded during transitions from glacial to interglacial conditions during MIS10-9 and MIS2-1 (Fig. 2C). A deglacial peak in $B/Ca_{P.\ wuellerstorfi}$ has been previously noted for MIS2-1 (Allen et al., 2015) and was attributed to changing CO_2 storage during the deglaciation at a deeper site.

3.3. Antarctic intermediate water paleoceanography since 400 ka

In order to assess paleoceanographic changes to AAIW in the late Pleistocene, we combine our results and newly tested proxies with other established indicators of water mass history, including benthic foraminiferal $\delta^{13}C$. Seawater $\delta^{13}C$ values result from differences in the source regions (from primary productivity and temperature-dependent fractionation during air–sea gas exchange; Lynch-Stieglitz et al., 1995), the age of the water mass, and productivity fluctuations along the water's flow path. Epifaunal *P. wueller-*

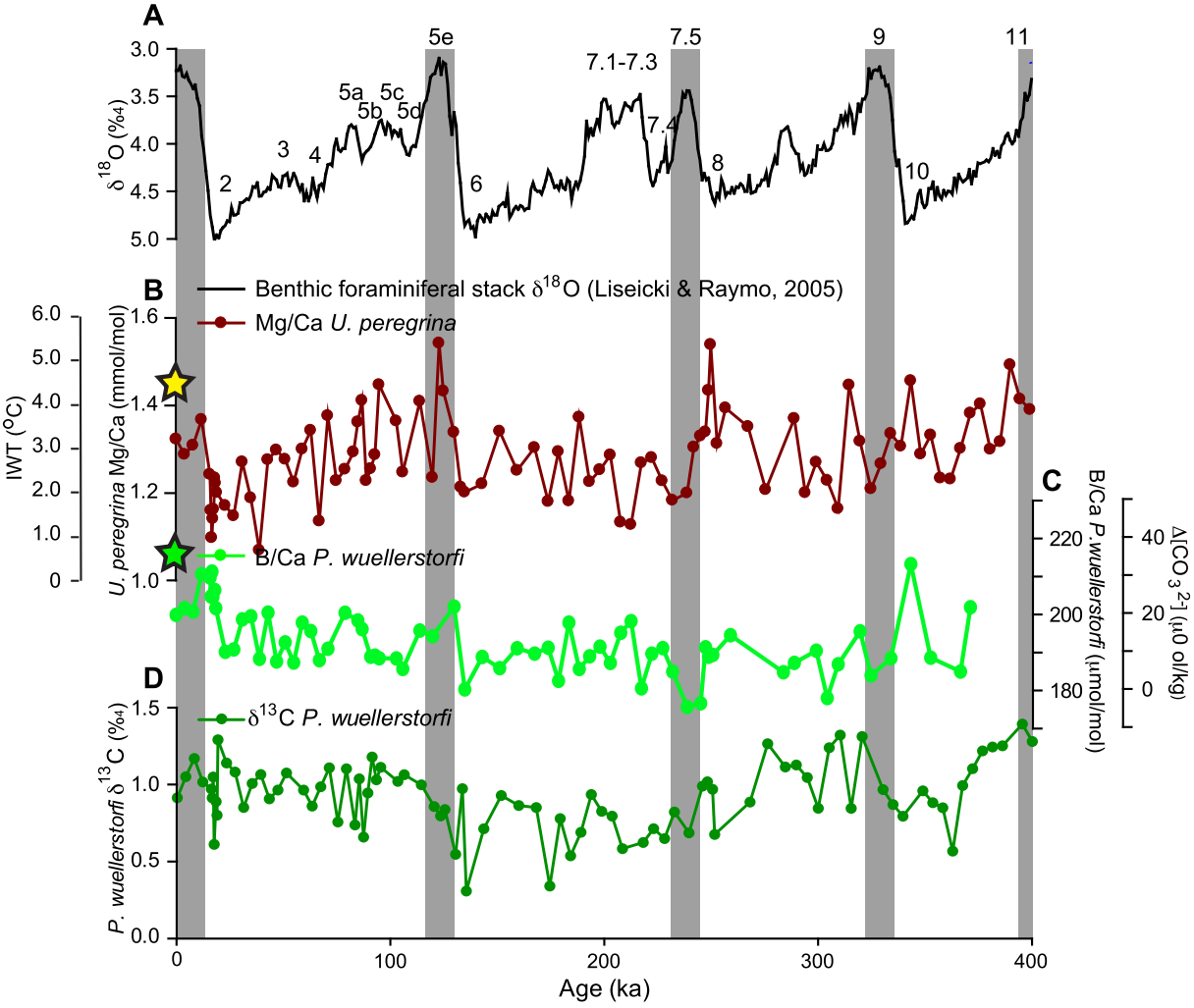

Fig. 4. Compilation of AAIW proxy records from DSDP593 A: benthic foraminiferal δ^{18}O LR04 stack (black; Lisiecki and Raymo, 2005), B: Mg/Ca$_{U.\ peregrina}$ (maroon), calculated as IWT according to Elderfield et al. (2010), C: B/Ca$_{P.\ wuellerstorfi}$ (light green), calculated as $\Delta[CO_3^{2-}]$ according to Rae et al. (2011), D: and $\delta^{13}C_{P.\ wuellerstorfi}$ (forest green). (For interpretation of the references to color in this figure, the reader is referred to the web version of this article.)

storfi have been shown to calcify without significant fractionation of carbon isotopes, providing an accurate record of bottom water δ^{13}C at the time of calcification (Curry and Oppo, 2005). In contrast, shallow infaunal *U. peregrina* have been suggested to calcify with a constant equilibrium offset of −0.90‰ with respect to bottom water δ^{13}C (Shackleton et al., 1984; Elderfield et al., 2012); however the offset is highly variable and may be driven by changes in pore water chemistry rather than bottom water chemistry (Zahn et al., 1986). The variability in the *P. wuellerstorfi* – *U. peregrina* offset is confirmed at DSDP593, ranging from 1.4 to 0.6‰. Benthic foraminiferal δ^{13}C values can additionally be affected by the flux of organic carbon to the core site, which is controlled by regional primary productivity and remineralization (Mackensen et al., 1993). Therefore, benthic foraminiferal δ^{13}C records also contain a localized signature of changing organic carbon flux and water mass remineralization potential at any one site. Allowing for these caveats, in certain settings benthic foraminiferal δ^{13}C has been used as a paleo-water mass tracer (e.g., Mackensen et al., 1993; Curry and Oppo, 2005; McCave et al., 2008; Bostock et al., 2010).

At DSDP593, $\delta^{13}C_{P.\ wuellerstorfi}$ values range from ∼ +0.6 to ∼ +1.4‰ from 400–0 ka, with generally lower values during the glacial stages; however, $\delta^{13}C_{P.\ wuellerstorfi}$ values remain ∼ +1.3‰ for the interval between MIS 5e and MIS 3 (Fig. 4D). Benthic foraminiferal $\delta^{13}C_{P.\ wuellerstorfi}$ values from DSDP593 are variable but are lower during the last two glacial intervals (MIS 6 and 2; Fig. 4D), suggesting possible decreased glacial ventilation and an increased southern source of AAIW (e.g., McCave et al., 2008; Pahnke and Zahn, 2005).

When compared with regional records of benthic foraminiferal δ^{13}C (MD97-2120; 1210 m water depth; Pahnke and Zahn, 2005; ODP1123; 3290 m water depth, bathed by CPDW; Elderfield et al., 2010), δ^{13}C values at the intermediate-depth sites (DSDP593 and MD97-2120) converge during interglacial stages, especially during the extreme interglacials of MIS 1, 5e, and 7.5 (yellow bars, Fig. 5B, C). Additionally, δ^{13}C values from deeper site ODP1123 also converge with the intermediate sites during these intervals (Fig. 5B, C). Similarity in δ^{13}C among different water depths during interglacials (MIS 1, 5e, 7.5) indicates that these sites were bathed by water masses with similar characteristics; given the location of these core sites (Fig. 1), this suggest similar δ^{13}C values in AAIW and CPDW, pointing to a similar source history during interglacials. A common source history for AAIW and CPDW during interglacials could be reflecting more vigorous North Atlantic Deep Water (e.g., Curry and Oppo, 2005), which contributes to both AAIW and CPDW through mixing in the Southern Ocean. Conversely, glacial stages (MIS 2, 4, 6, 8), and to some extent the more mild interglacials (MIS 3, 5a–c, 7.1–7.4), show a larger difference in δ^{13}C ($\Delta\delta^{13}C > 1.0$‰) between the shallowest core (DSDP593) and deepest core (ODP1123), with intermediate δ^{13}C values recorded in MD97-2120 (i.e., diverging δ^{13}C values), indicating dissimilar prop-

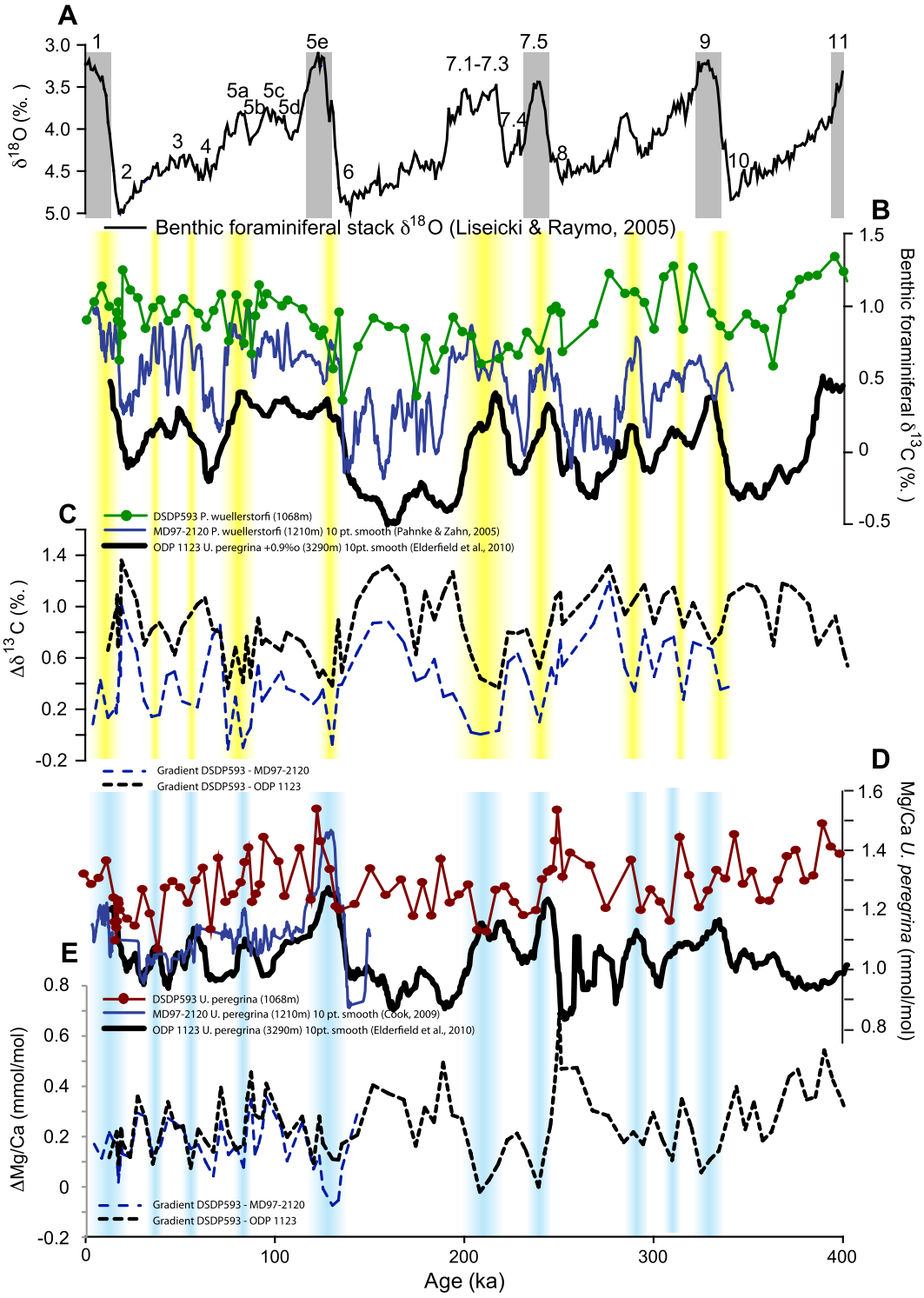

Fig. 5. Regional bottom water paleoceanographic records shown with A: LR04 benthic foraminiferal stack (black; Lisiecki and Raymo, 2005). Interglacial stages are highlighted by grey bars. B: Benthic foraminiferal $\delta^{13}C_{P.\ wuellerstorfi}$ records from DSDP593 (pink squares; this study), MD97-2120 (thin navy line; 10 pt. moving average; Pahnke and Zahn, 2005), and ODP1123 (thick black line; 10-pt moving average; Elderfield et al., 2010). C: The difference between benthic foraminiferal $\delta^{13}C$ from DSDP593 and MD97-2120 (navy dashed line), and DSDP593 and ODP1123 (black dashed line). Yellow bars in panels B and C highlight intervals with a small $\delta^{13}C$ gradient between shallower core DSDP593 (1068 m) and deeper core MD97-2120 (1210 m). D: Regional $Mg/Ca_{U.\ peregrina}$ records from DSDP593 (maroon circles; this study), MD97-2120 (thin navy line; 10-pt moving average; Cook, 2009), and ODP1123 (thick black line; 10-pt moving average; Elderfield et al., 2010). E: The difference between $Mg/Ca_{U.\ peregrina}$ records from DSDP593 and MD97-2120 (navy dashed line), and DSDP593 and ODP1123 (black dashed line). Blue bars in panels D and E highlight similar temperatures at shallower core DSDP593 (1068 m) and deeper core MD97-2120 (1210 m), where MD97-2120 data is not available (i.e. before 140 ka), blue bars represent decreased temperature gradient between DSDP593 and ODP1123 (3290 m). In panels C and E, 'differences' were calculated by smoothing previously published, higher resolution, data sets using a 5-point moving average, interpolating the smoothed records to ages in the DSDP593 data set, and subtracting the interpolated data from DSDP593 data. Similar timing of the yellow and blue bars represent intervals of similar $\delta^{13}C$ and Mg/Ca (temperature), respectively, indicating that AAIW and CPDW had similar properties during interglacials. (For interpretation of the references to color in this figure, the reader is referred to the web version of this article.)

erties between AAIW and CPDW. The glacial differences may be more indicative of regional heterogeneity in terms of source region, with greater Southern Ocean surface water contributing to AAIW.

Our $Mg/Ca_{U.\ peregrina}$ record from DSDP593 is the first paleotemperature record from this region that records purely AAIW and reveals glacial–interglacial scale changes since 400 ka, with warm interglacials and cooler glacials (Fig. 4B). Reconstructions of regional bottom water temperatures from $Mg/Ca_{U.\ peregrina}$ are also available from MD97-2120 (Cook, 2009) and ODP1123 (Elderfield et al., 2010) from the eastern side of New Zealand, affording the examination of the thermal structure of AAIW and CPDW using temperature from $Mg/Ca_{U.\ peregrina}$ as a conservative water mass tracer (Fig. 5C, D). Although the IWT record from $Mg/Ca_{U.\ peregrina}$ from MD97-2120 only extends from 120 to 0 ka, a pattern emerges whereby interglacial stages (MIS 1, 5e) have similar temperatures at all sites between 1068 m and 3290 m (blue bars; Fig. 5D, E). During glacial stages (MIS 2, 4, and 6) similar temperatures are recorded between MD97-2120 and deeper site ODP1123, while DSDP593 records a distinctly warmer temperature, suggesting that a glacial temperature gradient exists between 1068 m and 1210 m (Fig. 5D, E). This is consistent with the upper boundary of CPDW lying above MD97-2120 during the glacial stages, as was proposed by Pahnke and Zahn (2005).

The glacial–interglacial temperature trends extend beyond the available $Mg/Ca_{U.\ peregrina}$ data for MD97-2120 (by contrasting only data from DSDP593 and ODP1123) since interglacial stages MIS 7.5 and 9 showing similar paleotemperatures at DSDP593 and ODP1123 (Fig. 5D, E), whereas a larger temperature gradient is observed during glacial intervals (Fig. 5D, E). The modern temperature gradient between DSDP593 (modern temperature 4–5 °C) and ODP1123 (modern temperature 1.3 °C; Elderfield et al., 2010) is ~2.7–3.7 °C. This temperature gradient in the modern ocean would equate to a $Mg/Ca_{U.\ peregrina}$ difference of ~0.27–0.37 mmol/mol according to the Elderfield et al. (2010) equation, which approximates the Holocene gradients seen in our compilation (Fig. 5D, E).

There is a strong coincidence between the timing of intervals of similar water mass properties ($\delta^{13}C$ and paleotemperature) in the Southwest Pacific (yellow and blue bars, Fig. 5B–E) and the timing of interglacial stages from the Antarctic ice core deuterium temperature record (Petit et al., 1999), which indicates that our AAIW record is reflecting a wider, polar Southern Hemispheric signal. However, the heterogeneity of AAIW and CPDW does not strictly follow the typical saw-toothed pacing of glacial–interglacial cycles. MIS 3, which is often considered more glacial than interglacial in character, shows similar $\delta^{13}C$ values among the different water depths (Fig. 5B, C), but distinct $Mg/Ca_{U.\ peregrina}$ values between all 3 core sites (Fig. 5D, E). The substages MIS 7.1–7.3, which are interglacial-like according to global ice-volume and temperature (e.g., Lisiecki and Raymo, 2005), show similar values in both $\delta^{13}C$ and temperature (Fig. 5B–E). However, like substages MIS 7.1–7.3, a warmer interglacial-like interval (~270 ka) between the interglacial maxima of MIS 9 and glacial minima of MIS 8 also shows similar values in both $\delta^{13}C$ and temperature. In the Antarctic ice core record, temperature at 270 ka is warmer than MIS 3, and nearly as warm as MIS 7.1–7.3 (Petit et al., 1999). At DSDP593, MIS 8 is warmer than MIS 7.5, 5e, or 1 (Fig. 4), and may thus suggest a larger change in water mass source. Unlike other interglacial stages, MIS11 shows a large difference in $\delta^{13}C$ and temperature between DSDP593 and ODP1123, suggesting that this interglacial may have manifested differently than others (dotted black lines in Fig. 5C and E).

Regional comparison of both $\delta^{13}C$ and $Mg/Ca_{U.\ peregrina}$ show a difference in chemical (Fig. 5B, C) and thermal (Fig. 5D, E) property histories at each site, which is likely driven by ocean circulation. This is the case between the most extreme interglacials (MIS 1, 5e, 7.5, 9) and other interglacial stages (MIS 3, 5a–5d, 7.1–7.4). Due to the lower sample density afforded by DSDP593 (which is limited by sedimentation rate and sample availability), it is difficult to constrain the age models for some of the intervals (MIS 5a–5d, 7.1–7.4; Fig. 2). However, even by making large adjustments to the age model, the pattern of similar $\delta^{13}C$ among all sites during MIS 1, 5e and 7 cannot be eliminated (Fig. 5B–E). For example, using the existing age model, the period presumed to be 5a–5d shows a larger difference in $\delta^{13}C$ than during the glacial MIS 2 (Fig. 5B, C), while the temperature gradient seems to be larger during 5a–5d than during MIS 2 (Fig. 5D, E). Conversely, MIS 7.1–7.4 shows a larger intermediate-deep water gradient in $\delta^{13}C$ (Fig. 5B, C), and a smaller difference in temperature than during MIS 6 (Fig. 5D, E). Interestingly, the $\delta^{18}O_{P.\ wuellerstorfi}$ record from DSDP593 also shows disparity with the LR04 stack (Lisiecki and Raymo, 2005), with higher than expected $\delta^{18}O_{P.\ wuellerstorfi}$ during MIS 7.1–7.4 and during MIS 5b (Fig. 2). Therefore, these more moderate interglacial stages may have a reduced warming signal in the intermediate waters of the Southwest Pacific region relative to the deep waters, suggesting that the expression of interglacial sub-stages may be regionally dependent.

A previous study of MD97-2120 by Pahnke and Zahn (2005) suggested that the site recorded the base of AAIW, and may not have been bathed in AAIW during some glacial stages. At all times over the last 400 kyr, DSDP593 records higher $\delta^{13}C$ and warmer temperatures than site MD97-2120, indicating that DSDP593 is truly recording AAIW conditions for the duration (Fig. 5B–E). The broad similarity during interglacials in $\delta^{13}C$ and temperature characteristics between DSDP593 and MD97-2120 suggests that both sites are mainly recording changes in AAIW, without significant regional or productivity effects associated with their locations (Fig. 5B–E). However, during glacial stages, MD97-2120 $\delta^{13}C$ and temperature are more closely aligned with deep ODP1123 than with shallower intermediate DSDP593. As a result, if DSDP593 is always recording AAIW, this places the glacial boundary between AAIW and deep water masses between 1068 m and 1210 m, supporting the Pahnke and Zahn (2005) assertion that MD97-2120 sits on the lower boundary of AAIW for much of the past 400 kyr. During interglacials, DSDP593 and MD97-2120 are more closely aligned, indicating that the boundary between AAIW and deep water masses lies below 1210 m. Our reconstructed boundaries between AAIW and deep water masses are broadly consistent with reconstructions for the last deglaciation by McCave et al. (2008). Interestingly, the new data from DSDP593 confirms that this shift in water mass boundaries was a pervasive aspect of the last four glacial–interglacial cycles, and may be a persistent feature through the Pleistocene.

The $B/Ca_{P.\ wuellerstorfi}$ record presented herein is the first paleo-$\Delta[CO_3^{2-}]$ record for the Pacific Sector of the Southern Ocean over multiple glacial–interglacial stages and indicates a range in $B/Ca_{P.\ wuellerstorfi}$ from ~175 to ~215 μmol/mol, equivalent to $\Delta[CO_3^{2-}]$ −5 to 35 μg/kg, over the last 400 ka (Fig. 4C). While the resolution of our data is lower from 400–200 ka, we see evidence here that there has not been a significant long-term change in $\Delta[CO_3^{2-}]$ through this interval. Additionally, the last two glacial–interglacial transitions (MIS 6 to 5e and 2 to 1) both record an increase in $B/Ca_{P.\ wuellerstorfi}$, which could be interpreted as slightly more CO_2 being stored in the glacial intermediate Southern Ocean during glacials MIS 6 and 2 (Fig. 4C). This is because, assuming no change in oceanic alkalinity, an increase in dissolved CO_2 would decrease the proportion of dissolved inorganic carbon (DIC) present as $[CO_3^{2-}]$ (Zeebe and Wolf-Gladrow, 2001). A recent study by Allen et al. (2015) demonstrated increased storage of respired CO_2 in the deeper intermediate Southwest Pacific (~1600 m), supporting our assertion. Peaks in B/Ca during the last two deglacial transitions may represent abrupt periods of decreased CO_2 storage,

which has been noted for the last deglaciation (Allen et al., 2015), though our data is not of sufficient resolution to address these high-frequency variations. Due to the evidence that we present here for fluctuating $\Delta[CO_3^{2-}]$, further investigation is warranted for examining carbonate system changes in AAIW over previous glacial–interglacial cycles.

A record of $B/Ca_{P.\ wuellerstorfi}$ from the Atlantic sector of the Southern Ocean also illustrates glacial–interglacial scale changes during the last 800 kyr (Rickaby et al., 2010). As with our record (Fig. 4C), the Rickaby et al. (2010) record shows different trends among interglacials, with some interglacials recording higher B/Ca (MIS 1), and others recording low B/Ca (MIS 11). Thus, the fluctuations in B/Ca that we see suggest that there were changes in $\Delta[CO_3^{2-}]$ on glacial–interglacial timescales, and also within glacial and interglacial stages. While the large-scale last glacial maximum CO_2 storage reservoir was likely in the deep Southern Ocean (Burke and Robinson, 2012; Skinner et al., 2010), rather than the deep-Pacific (Broecker et al., 2004; Galbraith et al., 2007; Marchitto et al., 2005) some glacial storage of CO_2 in AAIW (e.g., Allen et al., 2015) is consistent with altered AAIW circulation and decreased ventilation suggested by previous $\delta^{13}C$ and radiocarbon studies (McCave et al., 2008; Bostock et al., 2010).

4. Conclusions

We have evaluated several methods for using foraminiferal geochemistry to reconstruct past changes in IWT and $\Delta[CO_3^{2-}]$ over the last 400 kyr, and demonstrate above that $Mg/Ca_{U.\ peregrina}$ and $B/Ca_{P.\ wuellerstorfi}$ are the best proxies for estimating paleotemperature and $\Delta[CO_3^{2-}]$, respectively. Using these new data, we present the first record of $Mg/Ca_{U.\ peregrina}$ for intermediate water depths over several glacial–interglacial cycles. The $Mg/Ca_{U.\ peregrina}$ data look dissimilar and show no correlation to $B/Ca_{P.\ wuellerstorfi}$ or $Mg/Ca_{P.\ wuellerstorfi}$, suggesting that $Mg/Ca_{U.\ peregrina}$ is not controlled by carbonate ion effects at intermediate water depths. Our $B/Ca_{U.\ peregrina}$ record from DSDP593 shows broadly different characteristics to the $B/Ca_{P.\ wuellerstorfi}$ record, suggesting that $B/Ca_{U.\ peregrina}$ cannot be used to reconstruct past changes in $\Delta[CO_3^{2-}]$ using presently available calibrations. Our new intermediate water records illustrate that late Pleistocene interglacial AAIW in the Southwest Pacific was characterized as warm and well-ventilated, and with similar properties to CPDW. Conversely, over the last 400 kyr, glacial stages had cooler and less ventilated AAIW, dissimilar in properties to CPDW. We place the glacial stage water mass boundary that separates AAIW from deeper water masses at between 1068 m and 1210 m in the Southwest Pacific, significantly shallower than the modern boundary at ~1500 m.

Acknowledgements

Funding for this research was provided by NERC awards NE/I027703/1 (E.L.M., S.K., H.E.) and IP-1339-1112 (E.L.M., A.C.E., S.K. and M.J.L.). We would like to thank Joanne Menegazzo, Hilary Sloane, and Jessica Bownes for analytical assistance; Tom Marchitto, Whitney Doss, James Rae, Will Gray, Katherine Allen, Tom Williams, Jo Kerr, and Jake Howe for helpful discussions. The manuscript was improved by comments from the Editor, Jean Lynch-Stieglitz, and two anonymous reviewers. This research used samples provided by the International Ocean Discovery Program (IODP) and we would like to thank the Kochi IODP Core Repository for help with core sampling. All previously unpublished data has been archived at: https://www.ncdc.noaa.gov/paleo/study/18918.

Appendix A. Supplementary material

Supplementary material related to this article can be found online at http://dx.doi.org/10.1016/j.epsl.2015.07.013.

References

Allen, K.A., Sikes, E.L., Honisch, B., Elmore, A.C., Guilderson, T., Rosenthal, Y., Anderson, B., 2015. Southwest Pacific deep water carbonate chemistry linked to high southern latitude climate and atmospheric CO_2 during the last glacial termination. Quat. Sci. Rev.

Anderson, R.F., Ali, A., Bradtmiller, L.I., Nielsen, S.H.H., Fleisher, M.Q., Anderson, B.E., Burckle, L.H., 2009. Wind-driven upwelling in the Southern Ocean and the deglacial rise in atmospheric CO_2. Science 323, 1441–1448.

Barker, S., Greaves, M., Elderfield, H., 2003. A study of cleaning procedures used for foraminiferal Mg/Ca paleothermometry. Geochem. Geophys. Geosyst. 4 (9), 1–20.

Basak, C., Martin, E.E., Horikawa, K., Marchitto, T., 2010. Southern Ocean source of ^{14}C-depleted carbon in the North Pacific during the last deglaciation. Nat. Geosci. 3, 770–773.

Bostock, H.C., Opdyke, B.N., Williams, M.J.M., 2010. Characterising the intermediate depth waters of the Pacific Ocean $\delta^{13}C$ and other geochemical tracers. Deep-Sea Res., Part 1, Oceanogr. Res. Pap. 57, 847–859.

Bostock, H.C., Barrows, T.T., Carter, L., Chase, Z., Cortese, G., Dunbar, G.B., Ellwood, M., Hayward, B., Howard, W., Neil, H.L., Noble, T.L., Mackintosh, A., Moss, P.T., Moy, A.D., White, D., Williams, M.J.M., Armand, L.K., 2013a. A review of the Australian-New Zealand sector of the Southern Ocean over the last 30 ka (Aus-INTIMATE project). Quat. Sci. Rev. 74, 35–57.

Bostock, H.C., Sutton, P.J., Williams, M.J.M., Opdyke, B.N., 2013b. Reviewing the circulation and mixing of Antarctic Intermediate Water in the South Pacific using evidence from geochemical tracers and Argo float trajectories. Deep-Sea Res., Part 1, Oceanogr. Res. Pap. 73, 84–98.

Broecker, W.S., Clark, E., Hajdas, I., Bonani, G., 2004. Glacial ventilation rates for the deep Pacific Ocean. Paleoceanography 19 (2), PA2002. http://dx.doi.org/10.1029/2003PA000974.

Burke, A., Robinson, J.F., 2012. The Southern Ocean's role in carbon exchange during the last deglaciation. Science 335 (6068), 557–561.

Cook, M.R., 2009. Antarctic Intermediate Water – Pacific Sector Variations over the past 150 ka. Doctoral Dissertation submitted to the University of Cambridge.

Cooke, P.J., Nelson, C.S., Crundwell, M.P., Field, B.D., Elkington, E.S., Stone, H.H., 2004. Textural variations in Neogene pelagic carbonate ooze at DSDP Site 593, southern Tasman Sea, and their paleoceanographic implications. N.Z. J. Geol. Geophys. 47 (4), 787–807.

Curry, W.B., Oppo, D.W., 2005. Glacial water mass geometry and the distribution of $\delta^{13}C$ and $\sum CO_2$ in the western Atlantic Ocean. Paleoceanography 20, 1–12.

Doss, W., 2014. Ph.D. thesis. University of Colorado, Boulder.

Dudley, W.C., Nelson, C.S., 1989. Quaternary surface-water stable isotope signal from calcareous nannofossils at DSDP Site 593, Southern Tasman Sea. Mar. Micropaleontol. 13, 353–373.

Elderfield, H., Yu, J., Anand, P., Kiefer, T., Nyland, B., 2006. Calibrations for benthic foraminiferal Mg/Ca paleothermometry and the carbonate ion hypothesis. Earth Planet. Sci. Lett. 250, 633–649.

Elderfield, H., Greaves, M., Barker, S., Hall, I.R., Tripati, A., Ferretti, P., Crowhurst, S., Booth, L., Daunt, C., 2010. A record of bottom water temperature and seawater $\delta^{18}O$ for the Southern Ocean over the past 440 kyr based on Mg/Ca of benthic foraminiferal Uvigerina spp. Quat. Sci. Rev. 29, 160–169.

Elderfield, H., Ferretti, P., Greaves, M., Crowhurst, S., McCave, I.N., Hodell, D., Piotrowski, A., 2012. Evolution of ocean temperature and ice volume through the mid-pleistocene climate transition. Science 337, 704.

Elmore, A.C., 2009. Late pleistocene changes in Northern component water: inferences from geochemical and sedimentological records from Gardar Drift. Ph.D. Dissertation. Rutgers University.

Galbraith, Eric D., Jaccard, Samuel L., Pedersen, Thomas F., Sigman, Daniel M., Haug, Gerald H., Cook, Mea, Southon, John R., Francois, Roger, 2007. Carbon dioxide release from the North Pacific abyss during the last deglaciation. Nature 449 (7164), 890–893.

Hall, I., McCave, I.N., Shackleton, N.J., Weedon, G.P., Harris, S.E., 2001. Intensified deep Pacific inflow and ventilation in Pleistocene glacial times. Nature 412, 802–812. http://dx.doi.org/10.1038/35090552.

Head, P.S., Nelson, C.S., 1994. A high-resolution oxygen isotope record for the past 6.4 million years at DSDP Site 593, Challenger Plateau, southern Tasman Sea. In: van der Lingen, G.J., Swanson, K.M., Muir, R.J. (Eds.), Evolution of the Tasman Sea Basin. A.A. Balkema, Rotterdam, pp. 159–179.

Herraiz-Borreguero, L., Rintoul, S.R., 2011. Regional circulation and its impact on upper ocean variability south of Tasmania. Deep-Sea Res., Part 2, Top. Stud. Oceanogr. 58, 2071–2081.

Kennett, J.P., von der Borch, C.C., et al., 1986. Site 593: Challenger Plateau. Initial reports of DSDP 90. U.S. Govt. Priting Office, Washington, pp. 55–156.

Lisiecki, L.E., Raymo, M.E., 2005. A Pliocene–Pleistocene stack of 57 globally distributed benthic $\delta^{18}O$ records. Paleoceanography 20, PA1003. http://dx.doi.org/10.1029/2004PA001071.

Lynch-Stieglitz, J., Stocker, T.F., Broecker, W.S., Fairbanks, R.G., 1995. The influence of air–sea exchange on the isotopic composition of oceanic carbon: observations and modeling. Glob. Biogeochem. Cycles 9 (4), 653–665.

Mackensen, A., Hubberten, H.-W., Bickert, T., Fischer, G., Futterer, D.K., 1993. The $\delta^{13}C$ in benthic foraminiferal tests of Fontbotia wuellerstorfi (Schwager) relative to the $\delta^{13}C$ of dissolved inorganic carbon in Southern Ocean deep water: implications for glacial ocean circulation models. Paleoceanography 8 (5), 587–610.

Marchitto, T.M., Lynch-Stieglitz, J., Hemming, S.R., 2005. Deep Pacific $CaCO_3$ compensation and glacial–interglacial atmospheric CO_2. Earth Planet. Sci. Lett. 231, 317–336.

Marchitto, T.M., Lehman, S.J., Ortiz, J.D., Fluckiger, J., van Green, A., 2007. Marine radiocarbon evidence for the mechanism of deglacial atmospheric CO_2 rise. Science 316, 1456–1459.

Marchitto, T.M., Curry, W.B., Lync-Stieglitz, J., Bryan, S.P., Cobb, K.M., Lund, D.C., 2014. Improved oxygen isotope temperature calibrations for cosmopolitan benthic foraminifera. Geochim. Cosmochim. Acta 130, 1–11.

Martin, P.A., Lea, D.W., Rosenthal, Y., Shackleton, N.J., Sarnthein, M., Papenfuss, T., 2002. Quaternary deep sea temperature histories derived from benthic foraminiferal Mg/Ca. Earth Planet. Sci. Lett. 198, 193–209.

McCave, I.N., Carter, L., Hall, I.R., 2008. Glacial–interglacial changes in water mass structure and flow in the SW Pacific Ocean. Quat. Sci. Rev. 27, 1886–1908.

Misra, S., Greaves, M., Owen, R., Kerr, J., Elmore, A.C., Elderfield, H., 2014. Determination of B/Ca of natural carbonates by HR-ICP-MS. Geochem. Geophys. Geosyst. 15 (4), 1617–1628.

Mulhearn, P.J., 1985. A deep hydrographic section across the Tasman Sea. Ranrl Technical Memorandum. Department of Defence, pp. 1–25.

Nelson, C.S., Hendy, C.H., Dudley, W.C., 1986. Quaternary isotope stratigraphy of hole 593, Challenger Plateau, South Tasman Sea: preliminary observations based on foraminifers and calcareous nannofossils. In: Initial Reports of the Deep Sea Drilling Project 90, pp. 1413–1424.

Nelson, C.S., 1986. Lithostratigraphy of Deep Sea Drilling Project Leg 90 drill sites in the southwest Pacific: an overview. In: Kennett, J.P., von der Borch, C.C., et al. (Eds.), Initial Reports of the Deep Sea Drilling Project 90. U.S. Government Printing Office, Washington, pp. 1471–1491.

Ostlund, H.G., et al., 1987. GEOSECS Atlantic, Pacific, and Indian Ocean Expeditions, vol. 7. NSF, Washington, DC.

Pahnke, K., Zahn, R., Elderfield, H., Schulz, M., 2003. 340,000-year centennial-scale marine record of southern hemisphere climatic oscillation. Science 301 (5635), 948–952.

Pahnke, K., Zahn, R., 2005. Southern hemisphere water mass conversion linked with North Atlantic climate variability. Science 307, 1741.

Petit, J.R., Jouzel, J., Raynaud, D., Barkov, N.I., Barnola, J.M., Basile, I., Bender, M., Chappellaz, J., Davis, J., Delaygue, G., Delmotte, M., Kotlyakov, V.M., Legrand, M., Lipenkov, V., Lorius, C., Pépin, L., Ritz, C., Saltzman, E., Stievenard, M., 1999. Climate and atmospheric history of the past 420,000 years from the Vostok Ice Core, Antarctica. Nature 399, 429–436.

Rae, J.W.B., Foster, G.L., Schmidt, D.N., Elliot, T., 2011. Boron isotopes and B/Ca in benthic foraminifera: proxies for the deep ocean carbonate system. Earth Planet. Sci. Lett. 302 (3–4), 403–413.

Raitzsch, M., Hathorne, E.C., Kuhnert, H., Groeneveld, J., Bickert, T., 2011. Modern and late Pleistocene B/Ca ratios of the benthic foraminifer Planulina wuellerstorfi determined with laser ablation ICP-MS. Geology 39 (11), 1039–1042.

Reid, J.L., 1997. On the total geostrophic circulation of the Pacific Ocean: flow patterns, tracers and transports. Prog. Oceanogr. 29, 263–352.

Rickaby, R.E.M., Elderfield, H., Roberts, N., Hillenbrand, C.-D., Mackensen, A., 2010. Evidence for elevated alkalinity in the glacial Southern Ocean. Paleoceanography 25 (1), PA1762.

Rohling, E., Grant, K., Bolshaw, M., Roberts, A.P., Siddall, M., Hemleben, Ch., Kicera, M., 2009. Antarctic temperature and global sea level closely coupled over the past five glacial cycles. Nat. Geosci. 2, 500–504. http://dx.doi.org/10.1038/natgeo557.

Schlitzer, R., 2002. Ocean data view. http://www.awi-bremerhaven.de/GEO/ODV.

Schrag, D.P., Adkins, J.F., McIntyre, K., Alexander, J.L., Hodell, D.A., Charles, C.D., McManus, J.F., 2002. The oxygen isotopic composition of seawater during the Last Glacial Maximum. Quat. Sci. Rev. 21 (1–3), 331–342.

Shackleton, N.J., Hall, M.A., Boersma, A., 1984. Oxygen and carbon isotope data from leg 74 foraminifers. In: Blakeslee, J.H., Lee, M. (Eds.), Initial Reports of the Deep Sea Drilling Program, 74. U.S. Govt. Printing Office, Washington, pp. 599–612.

Talley, L.D., 1999. In: Webb, C., Keigwin, L.D. (Eds.), Mechanisms of Global Climate Change at Millennial Time Scales. In: Geophys. Monogr. Ser., vol. 112, pp. 1–22.

Williams, D.F., Ehrlich, R., Spero, H.J., Healy-Williams, N., Gary, A.C., 1988. Shape and isotopic differences between conspecific foraminiferal morphotypes and resolution of paleoceanographic events. Palaeogeogr. Palaeoclimatol. Palaeoecol. 64, 153–162.

Yu, J., Elderfield, H., 2007. Benthic foraminiferal B/Ca ratios reflect deep water carbonate saturation state. Earth Planet. Sci. Lett. 258 (1–2), 73–86.

Yu, J., Elderfield, H., 2008. Mg/Ca in the benthic foraminifera Cibicidoides wuellerstorfi and Cibicidoides mundulus: temperature versus carbonate ion saturation. Earth Planet. Sci. Lett. 276 (1–2), 129–139.

Zahn, R., Winn, K., Sarnthein, M., 1986. Benthic foraminiferal $\delta^{13}C$ and accumulation rates of organic carbon: uvigerina peregrina group and Cibicidoides wuellerstorfi. Paleoceanography 1 (1), 24–42.

Zeebe, Richard E., Wolf-Gladrow, Dieter A., 2001. CO_2 in Seawater: Equilibrium, Kinetics, Isotopes, vol. 65. Gulf Professional Publishing.